JOURNAL OF GUIDANCE, CONTROL, AND DYNAMICS
Vol. 29, No. 4, July–August 2006

In-Plane Payload Capture with an Elastic Tether

Paul Williams*
Royal Melbourne Institute of Technology, Melbourne, Victoria 3083, Australia

The capture of payloads using tethers is a challenging task from a control point of view. In previous studies on coplanar capture, the precapture control design has been achieved by assuming that the tether is inextensible. However, the effect of tether longitudinal vibrations can cause errors in the position and velocity of the tether tip. Furthermore, the extra mass at the tip of the tether can induce longitudinal vibrations with significant amplitude that ultimately cause the tether to become slack. A guidance scheme based on optimal control methodology that can achieve rendezvous with a payload using a longitudinally flexible tether is demonstrated. Rather than treating the precapture and postcapture phases separately, an integrated control scheme is developed that successfully guides the tether to achieve rendezvous with a payload and then simultaneously damps the tether librations and longitudinal vibrations. Closed-loop performance of the system is demonstrated using a receding-horizon control strategy.

Nomenclature

$\boldsymbol{A}$	=	system state influence matrix
$\boldsymbol{B}$	=	system control influence matrix
D_{kj}	=	entries of pseudospectral differentiation matrix
EA	=	tether longitudinal stiffness
$\boldsymbol{f}$	=	right-hand side of system state equations
J	=	cost function in optimal control problem
$\boldsymbol{K}$	=	state feedback gain matrix
L	=	Lagrangian of tether system
$\mathcal{L}$	=	Bolza cost functional
L_f	=	reference tether length
L_N	=	Nth degree Legendre polynomial
l_0	=	unstrained tether length
m	=	total system mass, $m_1^0 + m_2$
m_p	=	payload mass
m_t	=	deployed tether mass, ρl_0
m_1	=	mother satellite mass, $m_1^0 - m_t$
m_2	=	mass of payload capture device
m_1^0	=	mother satellite mass before deployment of tether
m^*	=	reduced system mass, $(m_1 + m_t/2)(m_2 + m_t/2)/m - m_t/6$
$\bar{m}$	=	$m_1(m_2 + m_t)/m$
N	=	degree of approximating polynomial used in pseudospectral method
$\boldsymbol{Q}$	=	state weighting matrix in receding-horizon control law
Q_j	=	generalized forces in Lagrange's equations
R	=	orbit radius of tether system center of mass
$\boldsymbol{R}$	=	control weighting matrix in receding-horizon control law
R_p	=	orbit radius of payload
r_2	=	distance from tether system center of mass to tether tip
$\boldsymbol{S}_f$	=	terminal state weighting matrix in receding-horizon control law
T	=	horizon length in receding-horizon controller
$T_{\min}$	=	minimum tension level
t	=	time
t_f	=	final time
t_0	=	initial time
t_1	=	capture or event time
$\boldsymbol{u}$	=	system control vector
w_k	=	Legendre–Gauss–Lobatto quadrature weights
$\boldsymbol{x}$	=	system state vector
$\bar{\boldsymbol{x}}$	=	reference system states
$\delta\boldsymbol{u}$	=	perturbed control vector
$\delta\boldsymbol{x}$	=	perturbed state vector
ε	=	tether longitudinal strain
ε_r	=	reference static strain following payload capture
θ	=	in-plane libration angle
Λ_0	=	nondimensional unstrained tether length
μ	=	gravitational constant of the Earth
ρ	=	tether line density
ω	=	orbital angular velocity of tether system
ω_p	=	orbit angular velocity of payload

I. Introduction

TETHERED space systems have attracted much attention in recent years because of the large number of applications for which they can be used.[1] Space transportation is still in the early stages of development, and ways of reducing mission costs to make space travel an affordable option for the public has been at the forefront of research. The cost of fuel/propellant is still one of the biggest motivators for looking toward more advanced technology such as space elevators[2] and space tethers.[3,4] Although the technology for realizing exotic concepts such as the space elevator is still far from reality, the technology behind space tethers is well established by numerous flight tests and extensive theoretical work.[5–7] Some of the exciting applications of tethered satellite systems are electrodynamic propulsion,[8–11] payload boost[12–15] or deboost[16,17] via momentum transfer, aerobraking,[18] and high-altitude atmospheric studies.[19,20] The use of tethers for capturing operational or inoperational satellites and other space debris is a very useful and important application. The captured space debris could be used as ballast mass for more advanced momentum-exchange architectures,[21] deorbited to burn in the atmosphere, or boosted into a higher orbit (operational satellites). Regardless of the ultimate application, the problem of rendezvousing and capturing another object at the tip of a long tether is a very important astrodynamical problem.

The use of tethers for performing payload capture has been studied previously for capture in the orbital plane,[22–25] as well as capture in small relative inclination orbits.[26] Tether-mediated orbital rendezvous was first mentioned by Carroll[27] for cooperative rendezvous between the tether tip and the space shuttle. Carroll[28] later provided a preliminary design for a tether transport facility capable of providing between 0.9- and 1.2-km/s velocity increments to payloads. In this work, a slowly spinning tether configuration was used and techniques for mitigating the tension waves created by capturing and releasing payloads through tether reeling were discussed.

Received 1 May 2005; revision received 4 July 2005; accepted for publication 11 July 2005.

*Research Fellow, P.O. Box 71, School of Aerospace, Mechanical, and Manufacturing Engineering, Bundoora; paul.williams@rmit.edu.au. Member AIAA.

Stuart[22] originally considered in-plane cooperative tether-mediated rendezvous between a free-flying spacecraft and the tether tip by combining tether reeling with thrusters on the tether tip. In this work, however, the tether reel dynamics were not directly considered and the nominal tether length was limited to 10 km. Stuart[22] gave consideration to both minimum-fuel and maximum-rendezvous time trajectories. Maximum-time trajectories were calculated by matching the tether tip and payload positions and velocities at an instant then releasing the tether tension. More recently, Blanksby and Trivailo[23] devised a method for achieving a gentle rendezvous for the in-plane case using tension control. A simpler control technique was suggested by Williams et al.[24,25] by employing a nonlinear receding-horizon tracking controller. In this approach, the tether tip is maneuvered from an arbitrary initial state to a unique libration cycle that ensures rendezvous at the rendezvous time. The ability to extend the rendezvous time by using an actuator mass was investigated by Williams and Blanksby.[29] It was found that, by using a tether extended well beyond the orbit of the payload, proximity times on the order of 9 min can be achieved. Westerhoff[30] discussed a linear control strategy to minimize errors in rendezvous for a spinning momentum-exchange system assuming that the tether is positioned reasonably close to the desired rendezvous position. It was assumed that errors in the out-of-plane direction could be handled by thrusters on the payload. Williams[26] studied the capture of noncooperative payloads that are in inclined orbits relative to the tether system, requiring that capture take place out-of-plane with respect to the tether system orbit. Optimal control methodology was used to determine open-loop trajectories for an inextensible tether.

In most studies of the rendezvous maneuver, the tether has been modeled as a rigid inextensible rod. Furthermore, the addition of a mass at the tip of the tether introduces longitudinal vibrations that, when coupled with the librational dynamics, can cause the tether to become slack. In Ref. 24, Williams et al. studied both phases of the capture scenario, but employed different dynamic models of the tether for precapture and postcapture control. The assumption of a rigid-rod tether neglects the tether longitudinal extension, which can cause tens to hundreds of meters position error for the tether tip. The purpose of this paper is to study the rendezvous and capture of payloads in the orbital plane with an elastic tether. Rather than separating the capture and postcapture control phases, an integrated strategy is proposed that determines the optimal open-loop controls for a complete capture maneuver. The approach is demonstrated for a baseline case where the tether is maneuvered from an initial radial-pointing configuration to capture a 1000-kg payload with zero relative position and velocity. The system is then controlled to return to its original radial pointing position. In addition to this, a new receding-horizon control strategy is developed for tracking the time-varying reference trajectories to provide closed-loop control of the system dynamics.

II. Mathematical Model

The tether system is modeled as two point masses connected via a straight elastic tether, assumed to be uniform in mass, as shown in Fig. 1. It is assumed that the system center of mass follows a Keplerian circular orbit. This assumption is reasonable if the total maneuver time is relatively short and if the payload mass is relatively small compared to the total system mass. For simplicity, only the in-plane motion of the system is considered. The Lagrangian for a flexible tether is given by

$$L = \tfrac{1}{2}m^* l_0^2(1+\varepsilon)^2(\dot\theta+\omega)^2 + \tfrac{1}{2}\bar m[\dot l_0(1+\varepsilon)+l_0\dot\varepsilon]^2$$
$$-\tfrac{1}{2}m^* l_0^2(1+\varepsilon)^2\omega^2(1-3\cos^2\theta) - (EA/2)l_0\varepsilon^2 \tag{1}$$

where $\bar m = m_1(m_2+m_t)/m$, $m_1 = m_1^0 - m_t$ is the mother satellite mass, m_2 is the subsatellite mass, and ω is the orbital angular velocity of the system center of mass.

The equations of motion may be derived by a straightforward application of Lagrange's equations,

$$\frac{\mathrm{d}}{\mathrm{d}t}\left(\frac{\partial L}{\partial \dot q_j}\right) - \frac{\partial L}{\partial q_j} = Q_j \tag{2}$$

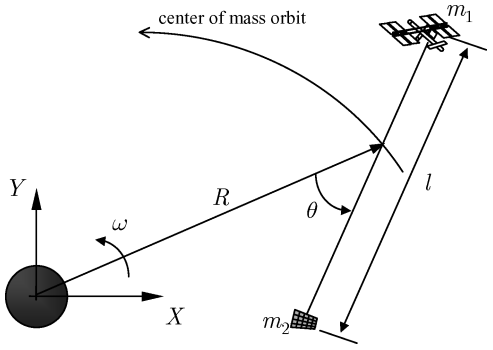

Fig. 1 Simplified model of flexible tethered satellite system.

The resulting equations may be written in the nondimensional form,

$$\theta'' + 2\left[\frac{m_1(m_2+m_t/2)}{mm^*}\frac{\Lambda_0'}{\Lambda_0} + \frac{\varepsilon'}{1+\varepsilon}\right](\theta'+1)$$
$$+3\sin\theta\cos\theta = 0 \tag{3}$$

$$\varepsilon'' + \frac{\Lambda_0''}{\Lambda_0}(1+\varepsilon) + 2\frac{\Lambda_0'}{\Lambda_0}\varepsilon' + \frac{(2m_1-m)m_t}{m_1(m_2+m_t)}\frac{\Lambda_0'}{\Lambda_0}\left[\frac{\Lambda_0'}{\Lambda_0}(1+\varepsilon)+\varepsilon'\right]$$
$$-\left[\frac{(m_1+m_t/3)(m_2+m_t/3)-m_t^2/36}{m_1(m_2+m_t)}\right]$$
$$\times(1+\varepsilon)[(\theta'+1)^2+(3\cos^2\theta-1)] = -\frac{EA}{L_f\Lambda_0\bar m\omega^2}\varepsilon \tag{4}$$

where $\Lambda_0 = l_0/L_f$ is the nondimensional unstrained tether length and $(\,)' = \mathrm{d}(\,)/\mathrm{d}(\omega t)$ is the nondimensional time derivative. The control input is assumed to be the reel acceleration Λ_0'', and hence, the equations of motion can be expressed in the following state-space form:

$$x_1' = x_2$$

$$x_2' = -2\left[\frac{\left(m_1^0-\rho x_5 L_f\right)(m_2+\rho x_5 L_f/2)}{\left(m_1^0-\rho x_5 L_f/2\right)(m_2+\rho x_5 L_f/2)-\left(m_1^0+m_2\right)\rho x_5 L_f/6}\right.$$
$$\left.\times\frac{x_6}{x_5}+\frac{x_4}{1+x_3}\right](x_2+1) - 3\sin x_1\cos x_1$$

$$x_3' = x_4$$

$$x_4' = -\frac{u}{x_5}(1+x_3) - 2\frac{x_6}{x_5}x_4 - \frac{\left(m_1^0-m_2-2\rho x_5 L_f\right)\rho x_5 L_f}{\left(m_1^0-\rho x_5 L_f\right)(m_2+\rho x_5 L_f)}\frac{x_6}{x_5}$$
$$\times\left[\frac{x_6}{x_5}(1+x_3)+x_4\right]$$
$$+\left[\frac{\left(m_1^0-2\rho x_5 L_f/3\right)(m_2+\rho x_5 L_f/3)-(\rho x_5 L_f)^2/36}{\left(m_1^0-\rho x_5 L_f\right)(m_2+\rho x_5 L_f)}\right]$$
$$\times(1+x_3)\left[(x_2+1)^2+\left(3\cos^2 x_1-1\right)\right]$$
$$-\frac{EA\left(m_1^0+m_2\right)}{L_f x_5\left(m_1^0-\rho x_5 L_f\right)(m_2+\rho x_5 L_f)\omega^2}x_3$$

$$x_5' = x_6$$

$$x_6' = u \tag{5}$$

where $(x_1, x_2, x_3, x_4, x_5, x_6) = (\theta, \theta', \varepsilon, \varepsilon', \Lambda_0, \Lambda_0')$ are the system state variables. Equation (5) is highly nonlinear and coupled in both

the states and control. The potential instability of the tether librations and tether strain is evident by examining the coefficients of θ' in Eq. (3) and the coefficients of ε' in Eq. (4). When the tether length rate is negative, the damping terms in the strain and libration equations are negative, and hence, the librations and longitudinal vibrations are unstable. These phenomena are the cause of the well-known instability of the system during retrieval unless suitable control methods are used.[31] In fact, for controlling the rendezvous maneuver, these terms in the equations of motion are essential for manipulating the longitudinal and librational dynamics.

III. Rendezvous Conditions

A. Zero Relative Position/Velocity Rendezvous

To rendezvous with a payload at the tip of a long tether requires that the tether tip be in the correct position at a specified time. Furthermore, it is desirable to minimize the difference in velocity between the tether tip and the payload to minimize the impulse applied at the tip of the tether. The transfer of momentum can cause string-like vibrations to be initiated, and although these can be damped by moving the tether attachment point,[32] it is preferable to achieve a gentle rendezvous. Naturally, errors in the tether rotational velocity cause errors in the relative capture velocity. Errors in the tether length cause not only position errors, but also errors in the relative capture velocity. Hence, it is crucial that the tether tip be in the right location at the rendezvous time to ensure that capture can take place.

The general rendezvous scenario is shown in Fig. 2. The tether system is in an orbit of radius R and uniform angular velocity ω. The payload is assumed to be in an orbit of radius R_p and uniform angular velocity ω_p. The position and velocity of the tether tip in the rotating orbital coordinates (x, y) centered at O may be obtained by first writing the position of the tether tip as

$$\boldsymbol{r}_{\text{tip}} = (R - r_2 \cos\theta)\boldsymbol{i} - r_2 \sin\theta \boldsymbol{j} \tag{6}$$

where $(\boldsymbol{i},\boldsymbol{j})$ are unit vectors in the directions of (x, y), respectively, and

$$r_2 = [(m_1 + m_t/2)/m] l_0 (1 + \varepsilon) \tag{7}$$

is the distance of the tether tip from the system center of mass. Differentiation of Eq. (6) gives the inertial velocity of the tether tip in orbital coordinates,

$$\boldsymbol{v}_{\text{tip}} = [-\dot{r}_2 \cos\theta + r_2(\dot{\theta} + \omega)\sin\theta]\,\boldsymbol{i} + [R\omega - \dot{r}_2 \sin\theta - r_2(\dot{\theta} + \omega)\cos\theta]\boldsymbol{j} \tag{8}$$

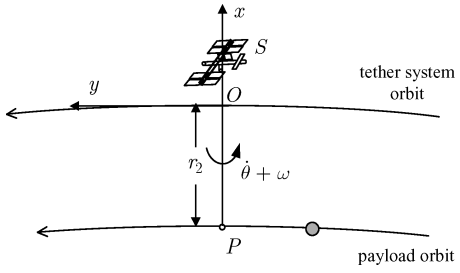

a)

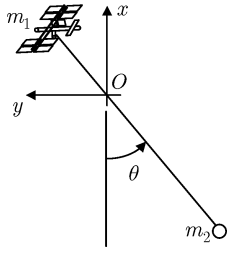

b)

Fig. 2 Rendezvous scenario: a) rendezvous Cooordinate system and b) tether system coordinates.

The conditions imposed for an instantaneous rendezvous are that the rendezvous takes place at the local vertical when the relative separation distance between the tether system and the payload is at a minimum. Hence, the tether libration angle must be zero. At this instant, the radial component of the relative velocity is zero. At the instant of rendezvous, the payload has a velocity of

$$\boldsymbol{v}_p = 0\boldsymbol{i} + R_p \omega_p \boldsymbol{j} \tag{9}$$

Equating the components of Eqs. (8) and (9) leads to the required rendezvous conditions for a flexible tether,

$$r_2 = R - R_p \tag{10}$$

$$\dot{r_2} = [(m_1 + m_t/2)/m] l_0 \dot{\varepsilon} + (m_1/m)\dot{l}_0(1 + \varepsilon) = 0 \tag{11}$$

$$\dot{\theta} = (R\omega - R_p\omega_p)/r_2 - \omega \tag{12}$$

These equations may be expressed in the more convenient nondimensional form by noting that

$$\omega = \sqrt{\mu/R^3}, \qquad \omega_p = \sqrt{\mu/R_p^3} \tag{13}$$

In nondimensional form, the conditions for a zero relative position/velocity rendezvous are

$$\theta = 0 \tag{14}$$

$$[(m_1 + m_t/2)/m]\Lambda_0(1 + \varepsilon) = (R - R_p)/L_f \tag{15}$$

$$[(m_1 + m_t/2)/m]\Lambda_0 \varepsilon' + (m_1/m)\Lambda_0'(1 + \varepsilon) = 0 \tag{16}$$

$$\theta' = [1/(R - R_p)]\left[R - \sqrt{R^3/R_p}\right] - 1 \approx -1.5 - 3\Delta h/(8R) - 5(\Delta h)^2/(16R^2) \tag{17}$$

where $\Delta h = R - R_p$. In other words, the required nondimensional libration rate given in Eq. (17) is a function of the orbital radii of the tether system and payload only. The required tether length, as determined from Eq. (15), is a function of the difference in the orbital altitudes of the tether system and payload. However, some important points must be made about these conditions. The rendezvous conditions for an inextensible tether do not provide any degree of freedom with respect to the tether length and length rate (see Ref. 24). For example, the length of inextensible tether must exactly match the required distance, and the inextensible length rate must be zero. In contrast, the length of the tether at rendezvous for a flexible tether is a function of the deployed tether length as well as the tether strain. In addition, the radial component of the tether velocity is a function of both the tether strain rate and the tether deployment rate. Hence, rather than imposing the strict requirement that both the strain rate and deployment rate be simultaneously zero at rendezvous, which is a sufficient condition, we can impose a more relaxed requirement that Eq. (16) be satisfied. This formulation, as will be seen later in this paper, aids in controlling the postcapture dynamics of the tether.

B. Capture Requirements in Low Earth Orbit

The requirements for capturing payloads in low Earth orbit can be determined numerically from Eqs. (14–17). Equation (17) suggests that the required nondimensional libration rate for payload capture is nearly constant for all practical separation distances because $\Delta h \ll R$. If higher-order terms are included, however, the required nondimensional libration rate varies linearly for small separation distances with a slope of -5.45×10^{-5}/km of separation for a tether system in an orbit with a radius of 6878 km. For a tether length of 100 km, the required nondimensional libration rate is approximately -1.5055.

An extremely important restriction to the precapture maneuver is that the tether be kept in tension. If the longitudinal oscillations are neglected, then there is a maximum amplitude libration cycle and, therefore, a maximum nondimensional libration rate that can

be achieved before the tether becomes slack. The maximum amplitude of the tether librations is approximately 66.5 deg (Ref. 33), which corresponds to a nondimensional libration rate of approximately 1.686. In other words, if the libration cycle is characterized by maximum libration rates of less than 1.686, then the tether will remain in tension. It is clear from Eq. (17) that this requirement is satisfied for all practical capture scenarios. For example, for the libration cycle to exceed this limit requires a separation distance of more than 2400 km. This is an extremely important result because it demonstrates that for a tether system and payload in circular orbits the tether does not have to rotate to achieve capture.

IV. Postcapture Dynamics

If the capture maneuver is successful, then the mass at the tip of the tether increases by an amount equal to the captured mass m_p. The equilibrium strain for the tether in its nominal pointing configuration is given by

$$\varepsilon_0 = 3\left[\frac{(m_1 + m_t/3)(m_2 + m_t/3) - m_t^2/36}{m_1(m_2 + m_t)}\right] \Bigg/ \left\{\left[\frac{EA}{L_f \Lambda_0 \bar{m}\omega^2} - 3\left[\frac{(m_1 + m_t/3)(m_2 + m_t/3) - m_t^2/36}{m_1(m_2 + m_t)}\right]\right\} \tag{18}$$

This equation illustrates that an increment in the mass at the tether tip, m_2, causes the value of the equilibrium strain to increase. Because the tether strain at the moment of capture is likely to be quite different from the equilibrium strain, the tether will begin vibrating longitudinally at an amplitude roughly equal to the difference between the strain at capture and the required equilibrium strain. If the strain vibration amplitude is large enough, then the tether can become slack at the peak of its libration cycle when the natural tension is at its minimum. This is shown in Fig. 3, which shows the strain time history of a longitudinally flexible tether, $EA = 100{,}000$ N, after the addition of a mass at the tip of the tether. Two frequencies are evident in the longitudinal vibrations in Fig. 3. The high-frequency, low-amplitude vibrations are caused by the increment of a mass at the tether tip. The lower frequency vibrations are caused by the coupling between the longitudinal and librational dynamics.

These results clearly illustrate the need to control the longitudinal dynamics of the tether after payload capture has occurred. Naturally, the amplitude of the longitudinal vibrations is related to the size of the payload that is captured: the larger the payload, the larger the vibrations. Previous work has demonstrated the capability of damping the longitudinal vibrations by reeling of the tether.[24] However, the control in Ref. 24 considers only the longitudinal dynamics of the tether and does not control the tether librations after capture. In this research, the capability of damping the longitudinal modes in conjunction with damping of the tether librations is considered.

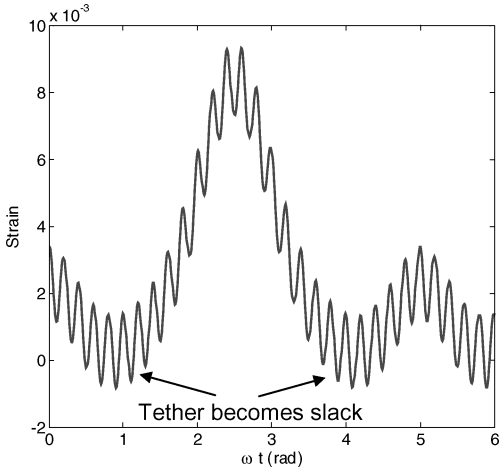

Fig. 3 Longitudinal dynamics of a flexible tether following payload capture.

V. Open-Loop Control for Pre- and Postcapture

A. Optimal Control Formulation

The guidance and control problem for maneuvering the tethered system can be stated in a general setting. There are many classes of problems that involve control switches, state switches, and other generalized events. In recent years, the optimization of such hybrid systems, that is, those that involve interactions between continuous and discrete dynamics has received some considerable attention.[34–38] Although the formulation of the rendezvous problem considered in this paper does not involve discrete dynamics, the multiple-phase nature of the problem gives rise to switches in the state dynamics as well as switches in the cost functional. For simplicity, the problem is formulated in a two-phase setting, although the approach is applicable to any number of phases. A complete treatment of the concepts discussed here may be found in Ref. 39.

The family of optimal control problems considered in this paper can be stated as follows: Find the state–control pair $\{\boldsymbol{x}(t), \boldsymbol{u}(t)\}$ over the time interval $[t_0, t_f] = I \subset \mathbb{R}$ that minimize the performance index

$$J = \int_{t_0}^{t_f} \mathcal{L}[\boldsymbol{x}(t), \boldsymbol{u}(t), t]\,\mathrm{d}t \tag{19}$$

subject to the nonlinear state equations,

$$\dot{\boldsymbol{x}}(t) = \begin{cases} \boldsymbol{f}^1[\boldsymbol{x}(t), \boldsymbol{u}(t), t] & t \in I^1 \\ \boldsymbol{f}^2[\boldsymbol{x}(t), \boldsymbol{u}(t), t] & t \in I^2 \end{cases} \tag{20}$$

the endpoint and event conditions,

$$\boldsymbol{e}_0[\boldsymbol{x}(t_0), t_0] = \boldsymbol{0} \tag{21}$$

$$\boldsymbol{e}_1\left[\boldsymbol{x}\left(t_1^-\right), \boldsymbol{x}\left(t_1^+\right), t_1\right] = \boldsymbol{0} \tag{22}$$

$$\boldsymbol{e}_f[\boldsymbol{x}(t_f), t_f] = \boldsymbol{0} \tag{23}$$

path constraints,

$$\boldsymbol{g}_L^1 \le \boldsymbol{g}_1[\boldsymbol{x}(t), \boldsymbol{u}(t), t] \le \boldsymbol{g}_U^1 \qquad t \in I^1$$

$$\boldsymbol{g}_L^2 \le \boldsymbol{g}_2[\boldsymbol{x}(t), \boldsymbol{u}(t), t] \le \boldsymbol{g}_U^2 \qquad t \in I^2 \tag{24}$$

and box constraints,

$$\boldsymbol{x}_L \le \boldsymbol{x}(t) \le \boldsymbol{x}_U$$

$$\boldsymbol{u}_L \le \boldsymbol{u}(t) \le \boldsymbol{u}_U \tag{25}$$

where $\boldsymbol{x} \in \mathbb{R}^{n_x}$ are the state variables, $\boldsymbol{u} \in \mathbb{R}^{n_u}$ are the control inputs, $t \in \mathbb{R}$ is the time,

$$\mathcal{L}[\boldsymbol{x}(t), \boldsymbol{u}(t), t] = \begin{cases} \mathcal{L}^1[\boldsymbol{x}(t), \boldsymbol{u}(t), t], & t \in I^1 \\ \mathcal{L}^2[\boldsymbol{x}(t), \boldsymbol{u}(t), t], & t \in I^2 \end{cases} \tag{26}$$

is the integrand of the Bolza cost function, $\mathcal{L}^k : \mathbb{R}^{n_{x^k}} \times \mathbb{R}^{n_{u^k}} \times \mathbb{R} \to \mathbb{R}$, $k = 1, 2$; $\boldsymbol{e}_0 \in \mathbb{R}^{n_{x^1}} \times \mathbb{R} \to \mathbb{R}^{n_{e^0}}$ are the initial point conditions; $\boldsymbol{e}_1 \in \mathbb{R}^{n_{x^1}} \times \mathbb{R}^{n_{x^2}} \times \mathbb{R} \to \mathbb{R}^{n_{e^1}}$ are the event conditions; $\boldsymbol{e}_f \in \mathbb{R}^{n_{x^2}} \times \mathbb{R} \to \mathbb{R}^{n_{e^f}}$ are the final point conditions; and $\boldsymbol{g}_{\mathrm{L,U}}^k \in \mathbb{R}^{n_{x^k}} \times \mathbb{R}^{n_{u^k}} \times \mathbb{R} \to \mathbb{R}^{n_{g^k}}$, $k = 1, 2$, are the lower and upper bounds on the path constraints. The time interval I is divided into two closed subintervals such that $I^1 = [t_0, t_1]$ and $I^2 = [t_1, t_f]$, where $I^1 \cap I^2 = \{t_1\}$ is the event time. At the event time, switches in the states, controls, and cost function are possible.

In general, the solution to such optimal control problems as just defined are not easy to obtain using standard approaches that rely on the formal derivation of the necessary conditions for optimality. Even much simpler two-point boundary-value problems are still regarded as being very difficult to solve.[40] The difficulties faced by formulating and solving multipoint boundary-value problems can be reduced greatly by employing so-called direct methods.[41] Direct methods transform the continuous-time problem into a discrete parameter optimization problem by using a discretization method to approximate the state equations and cost functional.

B. Direct Solution Method and Software

There are a number of efficient discretization methods for converting the continuous problem into a discrete one, some of which are described in Ref. 41. Most of the common methods used in practice employ sequential quadratic programming (SQP) algorithms to solve the underlying nonlinear programming problem (NLP). These methods are extremely efficient for solving even the most complex of problems. Some examples of different discretizations that can be used to convert the continuous problem are the Hermite–Simpson method (see Ref. 42), fifth-order Hermite–Legendre–Gauss–Lobatto (see Ref. 43), and pseudospectral methods.[44,45]

A general reusable software package for solving general single-phase optimal control problems, called DIRECT,[46] has been developed by the author. The package utilizes the MATLAB® environment to formulate the cost function, state equations, boundary conditions, and path constraints. The problem is automatically converted into an appropriate NLP depending on the selected discretization method. The NLP is solved using the sparse SQP software SNOPT,[47] originally coded in FORTRAN, but called from MATLAB via a mex-file interface. Default settings are used in SNOPT, and the Legendre pseudospectral discretization method (see Ref. 39) is used to obtain solutions in this work.

C. Application to Tethered Payload Capture

The basic concepts used to solve complex multiple-phase optimal control problems have been used to solve the specific problem of capturing a payload in low Earth orbit using tethers. Figure 4 shows the sequence of events that must take place in the proposed baseline scenario.

Initially, the tether is assumed to be in equilibrium with respect to longitudinal vibrations and in-plane librations. This is the nominal stationkeeping state for a tether system in a circular orbit. At some prescribed time t_0 before the rendezvous time t_1, tether reeling commences to "pump" the tether librational dynamics to the correct amplitude and phase that will enable a zero relative position/velocity rendezvous. Following capture of the payload, the tether is reeled to damp the tether librations as well as the longitudinal oscillations that develop from the addition of a mass at the tether tip. The tether returns to the stationkeeping configuration (with new equilibrium length) at time t_f.

The event point conditions defining the moment of rendezvous already have been derived. It now remains to specify the initial and final boundary conditions, as well as the form of the cost functional.

1. Initial Conditions

The initial configuration of the system before commencing the capture maneuver is the equilibrium position for the system. It is easy to verify that the librations are in equilibrium for

$$\theta(t_0) = 0, \qquad \theta'(t_0) = 0 \tag{27}$$

It is assumed that the amount of deployed tether is equal to the reference length and that the tether reel is initially locked,

$$\Lambda_0(t_0) = 1, \qquad \Lambda_0'(t_0) = 0 \tag{28}$$

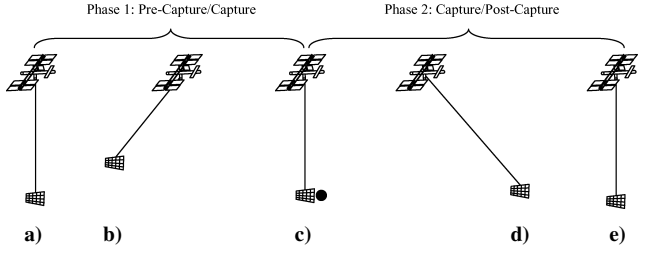

Fig. 4 Sequence of events for payload capture scenario, a) tether in equilibrium configuration, t_0; b) tether reeled-out and reeled-in to establish correct swing rate; c) rendezvous with payload at local vertical, t_1; d) tether reeled-out and reeled-in to damp librations and longitudinal waves, and e) tether returns to equilibrium configuration (t_f).

The tether strain rate is assumed to be initially zero and the initial tether strain is set so that the tether strain acceleration is zero, that is,

$$\varepsilon(t_0) = 1\Big/\Big(EA\Big/\Big\{3L_f\omega^2\Big[\big(m_1^0 - 2\rho L_f\big/3\big)(m_2 + \rho L_f/3) - \rho^2 L_f^2\big/36\Big]\Big/\big(m_1^0 + m_2\big)\Big\} - 1\Big) \tag{29}$$

$$\varepsilon'(t_0) = 0 \tag{30}$$

2. Final Conditions

The final boundary conditions at the time t_f are selected to be the same as the initial conditions, except that the final strain is not strictly enforced. Instead, the strain rate and strain acceleration are constrained to be zero. Hence, the final boundary conditions are given by

$$\theta(t_f) = 0, \qquad \theta'(t_f) = 0, \qquad \Lambda_0(t_f) = 1$$
$$\Lambda_0'(t_f) = 0, \qquad \varepsilon'(t_f) = 0, \qquad \varepsilon''(t_f) = 0 \tag{31}$$

Note that the strain acceleration is a complicated function of the states and control at the final time, as shown in Eq. (4).

3. Cost Function

The specification of the initial, event, and final conditions does not necessarily imply that the system will be well behaved on the trajectory between these points. As already noted, the longitudinal vibrations of the tether must be adequately suppressed following capture. In addition to this, it is desirable to ensure that the applied reel acceleration is smooth and minimal. Control of a longitudinally elastic tether can be sensitive to the cost function used for defining the system performance.[48] Instead of limiting the focus to one cost function, four different cost functions are considered. The rationale for this is that using only one cost function may lead to erroneous conclusions as to the requirements for the system. Hence, the following cost functions were selected for comparison:

$$J_1 := \begin{cases} \mathcal{L}^1 = (\Lambda_0'')^2, & t \in I^1 \\ \mathcal{L}^2 = 0.1(\Lambda_0'')^2 + 10(\varepsilon - \varepsilon_r)^2 + 10(\varepsilon')^2, & t \in I^2 \end{cases} \tag{32}$$

$$J_2 := (\Lambda_0'')^2 + 10(\varepsilon'')^2 + 100(\varepsilon')^2, \qquad t \in [I^1, I^2] \tag{33}$$

$$J_3 := \begin{cases} \mathcal{L}^1 = (\Lambda_0'')^2 + (\varepsilon'')^2, & t \in I^1 \\ \mathcal{L}^2 = (\varepsilon')^2 + (\varepsilon'')^2, & t \in I^2 \end{cases} \tag{34}$$

$$J_4 := (\varepsilon'')^2, \qquad t \in [I^1, I^2] \tag{35}$$

where ε_r is the reference static strain determined from Eq. (29) including the additional payload mass m_p value,

$$\varepsilon_r = 1\Big/\Big(EA\Big/\Big\{3L_f\omega^2\Big[\big(m_1^0 - 2\rho L_f\big/3\big)(m_2 + m_p + \rho L_f/3) - \rho^2 L_f^2\big/36\Big]\Big/\big(m_1^0 + m_2 + m_p\big)\Big\} - 1\Big) \tag{36}$$

Each cost function has a physically important meaning. For example, J_1 is defined differently in each phase. In the first phase, only the control input is penalized, whereas in the second phase the tether longitudinal dynamics are weighted more heavily than the control. The second cost, J_2, is defined identically in both phases and penalizes a combination of the control and the longitudinal dynamics. The third cost, J_3, penalizes a combination of the control and tether strain acceleration in the first phase, but penalizes only the tether longitudinal dynamics in the second phase. Finally, J_4 is identical in both phases and penalizes only the tether strain acceleration.

4. State Constraints

The importance of keeping the tether tension positive has been stressed in the preceding sections. Hence, it is necessary to ensure that the tension is kept positive in the open-loop maneuver. The tension can be kept positive by imposing a path constraint on the

tether strain as follows:

$$\varepsilon \geq T_{\min}/EA \tag{37}$$

where $T_{\min}$ is the minimum allowable tether tension.

VI. Feedback Control

The optimal open-loop trajectory can be sensitive to errors in the initial state, modeling errors, or external disturbances, and therefore, the open-loop control should be implemented with a feedback controller to provide good closed-loop performance. A proven approach for providing feedback control around time-varying reference trajectories is to linearize the system dynamics and solve a linear optimal control problem over a future finite horizon with the initial state equal to the current state (receding-horizon control).[49] An efficient approach for implementing receding-horizon control using pseudospectral methods was presented in Ref. 50, based on the work presented in Ref. 51. In this approach, the two-point boundary-value problem obtained by applying Pontryagin's maximum principle to the linear optimal control problem is discretized into a set of linear algebraic equations. A simpler and more efficient approach is used here to track the open-loop trajectories by formulating the discretized problem as a quadratic programming problem, for which analytical solutions are available. This has the advantage that less memory is required to obtain solutions and that a closed-form solution is available, rather than solving a large system of linear equations at each sample time.

Consider the problem of finding the controls $\delta\boldsymbol{u}(t)$ that minimize the quadratic performance index

$$\delta J = \frac{1}{2}\delta\boldsymbol{x}^{\top}(t+T)\boldsymbol{S}_f\delta\boldsymbol{x}(t+T) + \frac{1}{2}\int_t^{t+T}\left[\delta\boldsymbol{x}^{\top}(t)\boldsymbol{Q}\delta\boldsymbol{x}(t) + \delta\boldsymbol{u}^{\top}(t)\boldsymbol{R}\delta\boldsymbol{u}(t)\right]\mathrm{d}t^* \tag{38}$$

subject to the linearized state equations,

$$\delta\dot{\boldsymbol{x}} = \boldsymbol{A}(t)\delta\boldsymbol{x} + \boldsymbol{B}(t)\delta\boldsymbol{u} \tag{39}$$

the initial conditions,

$$\delta\boldsymbol{x}(t^* = t) = \boldsymbol{x}(t) - \bar{\boldsymbol{x}}(t) \tag{40}$$

and possibly the terminal constraints,

$$\delta\boldsymbol{x}(t^* = t+T) = 0 \tag{41}$$

where $\delta\boldsymbol{x} \in \mathbb{R}^{n_x}$ are the perturbed state variables, $\delta u \in \mathbb{R}^{n_u}$ are the perturbed controls, $\bar{\boldsymbol{x}} \in \mathbb{R}^{n_x}$ are the reference states, $\boldsymbol{A} \in \mathbb{R}^{n_x \times n_x}$ is the system state influence matrix, $\boldsymbol{B} \in \mathbb{R}^{n_x \times n_x}$ is the control influence matrix, $\boldsymbol{Q} \in \mathbb{R}^{n_x \times n_x}$ is a positive semidefinite weighting matrix that penalizes the deviations of the perturbed states, $\boldsymbol{R} \in \mathbb{R}^{n_u \times n_u}$ is a positive definite weight matrix that penalizes the deviations of the perturbed controls, and $\boldsymbol{S}_f \in \mathbb{R}^{n_x \times n_x}$ is a positive semidefinite terminal weight matrix that penalizes the deviations of the perturbed states at the end of the future horizon.

The linear optimal control problem may be discretized over the future horizon using a pseudospectral method.[51] If the time horizon is divided into $N+1$ nodes, and denoting the vector of unknown variables as

$$\boldsymbol{X} = [\delta\boldsymbol{x}(t_0), \delta\boldsymbol{x}(t_1), \ldots, \delta\boldsymbol{x}(t_N), \delta\boldsymbol{u}(t_0), \ldots, \delta\boldsymbol{u}(t_N)]^{\top} \tag{42}$$

then the discretized problem becomes one of finding the variables $\boldsymbol{X}$ to minimize the cost function

$$\delta\boldsymbol{J} = \frac{1}{2}\delta\boldsymbol{x}^{\top}(t_N)\boldsymbol{S}_f\delta\boldsymbol{x}(t_N) + \frac{T}{2}\sum_{k=0}^{N} w_k\left[\delta\boldsymbol{x}^{\top}(t_k)\boldsymbol{Q}\delta\boldsymbol{x}(t_k) + \delta\boldsymbol{u}^{\top}(t_k)\boldsymbol{R}\delta\boldsymbol{u}(t_k)\right] \tag{43}$$

subject to the constraints

$$\delta\boldsymbol{x}(t_0) = \delta\boldsymbol{x}(t)$$
$$\frac{2}{T}\sum_{j=0}^{N} D_{kj}\delta\boldsymbol{x}(t_j) - \boldsymbol{A}(t_k)\delta\boldsymbol{x}(t_k) - \boldsymbol{B}(t_k)\delta\boldsymbol{u}(t_k) = \boldsymbol{0} \qquad k = 0, \ldots, N \tag{44}$$
$$\delta\boldsymbol{x}(t_N) = \boldsymbol{0}$$

Equations (43) and (44) can be expressed in the matrix form

$$\delta J = \tfrac{1}{2}\boldsymbol{X}^{\top}\boldsymbol{H}\boldsymbol{X} \tag{45}$$

$$\boldsymbol{\mathcal{A}}\boldsymbol{X} = \boldsymbol{\mathcal{B}} \tag{46}$$

where $\boldsymbol{H}$ is the Hessian matrix defined by

$$\boldsymbol{H} = \begin{bmatrix} \frac{T}{2}w_0\boldsymbol{Q} & 0 & 0 & 0 & 0 & 0 & 0 \\ 0 & \frac{T}{2}w_1\boldsymbol{Q} & 0 & \vdots & \vdots & \vdots & \vdots \\ \vdots & 0 & \ddots & 0 & \vdots & \vdots & \vdots \\ \vdots & \vdots & 0 & \frac{T}{2}w_N\boldsymbol{Q} + \boldsymbol{S}_f & 0 & \vdots & \vdots \\ \vdots & \vdots & \vdots & 0 & \frac{T}{2}w_0\boldsymbol{R} & 0 & \vdots \\ \vdots & \vdots & \vdots & \vdots & 0 & \ddots & 0 \\ 0 & 0 & 0 & 0 & 0 & 0 & \frac{T}{2}w_N\boldsymbol{R} \end{bmatrix} \tag{47}$$

and where

$$\boldsymbol{\mathcal{A}} = \begin{bmatrix} \boldsymbol{I}_{n_x \times n_x} & 0 & 0 & 0 & 0 & 0 & 0 & 0 \\ \frac{2}{T}D_{0,0} - \boldsymbol{A}(t_0) & \frac{2}{T}D_{0,1} & \cdots & \frac{2}{T}D_{0,N} & -\boldsymbol{B}(t_0) & 0 & 0 & 0 \\ \frac{2}{T}D_{1,0} & \frac{2}{T}D_{1,1} - \boldsymbol{A}(t_1) & \ddots & \vdots & 0 & -\boldsymbol{B}(t_1) & 0 & 0 \\ \vdots & \ddots & \ddots & \frac{2}{T}D_{N-1,N} & 0 & 0 & \ddots & 0 \\ \frac{2}{T}D_{N,0} & \cdots & \frac{2}{T}D_{N,N-1} & \frac{2}{T}D_{N,N} - \boldsymbol{A}(t_N) & 0 & 0 & 0 & -\boldsymbol{B}(t_N) \\ 0 & 0 & 0 & \boldsymbol{I}_{n_x \times n_x} & 0 & 0 & 0 & 0 \end{bmatrix} \tag{48}$$

$$\boldsymbol{\mathcal{B}} = \begin{bmatrix} \delta\boldsymbol{x}(t) \\ 0 \\ \vdots \\ 0 \end{bmatrix} \tag{49}$$

where $D_{k,j} = \text{diag}[D_{kj}]_{n_x \times n_x}$ is a diagonal matrix, and

$$D_{kj} = \begin{cases} \dfrac{L_N(\tau_k)}{L_N(\tau_j)} \dfrac{1}{(\tau_k - \tau_j)} & k \neq j \\ -\dfrac{N(N+1)}{4} & k = j = 0, \quad w_k = \dfrac{2}{N(N+1)} \dfrac{1}{[L_N(\tau_k)]^2} \\ & \qquad k = 0, \ldots, N \\ \dfrac{N(N+1)}{4} & k = j = N \\ 0 & \text{otherwise} \end{cases} \tag{50}$$

Note that the nodes are selected as the Legendre–Gauss–Lobatto points and are defined on the interval $\tau \in [-1, 1]$, as described in Refs. 39 and 51.

The minimization of Eq. (45) with respect to $\boldsymbol{X}$ subject to the linear constraints (46) is a standard quadratic programming problem, which has the solution[52]

$$\boldsymbol{X}^* = \boldsymbol{H}^{-1}\boldsymbol{\mathcal{A}}^\top(\boldsymbol{\mathcal{A}}\boldsymbol{H}^{-1}\boldsymbol{\mathcal{A}}^\top)^{-1}\boldsymbol{\mathcal{B}} \tag{51}$$

This solution contains the discrete values of the states and controls at all node points. However, for feedback control, we are interested only in the value of the control at the initial point. Hence, by defining the row vector

$$\boldsymbol{V} = [\boldsymbol{0}_{n_u \times n_x(N+1)}, \boldsymbol{I}_{n_u \times n_u}, \boldsymbol{0}_{n_u \times n_u N}] \tag{52}$$

we obtain the state feedback control

$$\delta\boldsymbol{u}(t) = \boldsymbol{V}\boldsymbol{X}^* \triangleq \boldsymbol{K}(t; N, T)\delta\boldsymbol{x}(t) \tag{53}$$

where $\boldsymbol{K} \in \mathbb{R}^{n_u \times n_x}$ is a time-varying feedback gain matrix. It is apparent that Eq. (53) is a linear time-varying proportional feedback control law that can either be determined offline or online depending on the system complexity and level of discretization. In fact, it is possible to determine the feedback gain matrix treating T as the time to go to obtain neighboring optimal guidance, provided the original cost function for the nonlinear optimal control problem is expanded to second order. These options are not utilized here, but the general technique provides an extremely attractive alternative to integrating the matrix Riccati equation to obtain the same feedback gain matrix. In other words, this method does not require any explicit integration of differential equations for implementation.

Some additional important points regarding the implementation of the method need to be made. First, the Hessian matrix is a diagonal matrix, whose inverse is required in Eq. (51). Because this matrix does not change for a given application of the method, then it is necessary to only calculate this inverse once. This may be stored for later use. To take advantage of the fact that the Hessian and its inverse are diagonal, sparse matrices are used to store this information, speeding up the matrix calculations.

VII. Numerical Results

A representative system has been selected to demonstrate the performance of the proposed methods. The tether system is assumed to be in an orbit with a radius of 6878 km, and the payload is assumed to be in an orbit with a radius of 6778 km. The key properties of the tether system and payload are given in Table 1. The total maneuver time is assumed to be 12 rad, which is slightly less than two orbital revolutions of the tether system. Although the period of tether librations depends on amplitude, it varies between approximately 0.58 and 0.8 of one orbit, and so sufficient time is necessary to control the librational dynamics adequately. The precapture maneuver time must be at least on the order of the librational period. Therefore, the precapture phase is initiated 6 rad before capture, and another 6 rad is allowed for the tether to return to the stationkeeping phase. Note that this is a relatively short time interval and is selected because it is close to the period of librations, representing the upper level of possible performance for the system. Longer maneuver times are less demanding and, therefore, of less interest in this study.

Table 1 Example tether system properties

System property	Value
Main satellite mass	100,000 kg
Capture mechanism mass	500 kg
Tether density	10 kg/km
Tether stiffness	100,000 N
Nominal tether length	100 km
Payload mass	1,000 kg

A. Open-Loop Trajectory

The open-loop trajectory for the system described in Table 1 was determined with the minimum tension set to $T_{\min} = 0.5$ N. The Legendre pseudospectral method was used with the initial guess of the trajectory given by the tether equilibrium position with zero control input. The problem was discretized with 200 nodes on each phase, that is, 400 nodes in total. This number was selected to capture the longitudinal dynamics of the tether adequately. The accuracy of the discretized solution was assessed by propagating the discretized control input (interpolated with cubic splines) using ode45 in MATLAB with absolute and relative error tolerances set to 10^{-12}. If the discrete states match the propagated solution, then the solution is a feasible one. Solutions were obtained on a Pentium M laptop in MATLAB 7.0 in approximately 5 min. Because the solutions from the propagated solution match those obtained from DIRECT and are indistinguishable at the level of the plot, only the direct solutions are shown in the figures that follow.

The open-loop trajectories are shown in Figs. 5–12. The tether libration angle is shown in Fig. 5, which shows the relatively large libration amplitude that is required to generate the correct velocity for the tether tip. The maximum angle is approximately 61.2 deg. The corresponding libration rate is shown in Fig. 6. Figures 5 and 6 show the symmetrical nature of the librational dynamics for the proposed payload capture maneuver and the effectiveness of using tether reeling to pump and damp the librations in under two orbits. It is also clear that the choice of the performance index does not have a large effect on the tether librational dynamics for this maneuver. The tether strain and strain rate are shown in Figs. 7 and 8, respectively. Figure 8 begins to illustrate the differences in the choice of performance index. Although the initial conditions are the same for each case, there are some distinct differences in the strain variation at the beginning of the maneuver. The trajectory corresponding to J_1 has some oscillations in the strain, which are the largest in amplitude compared to the trajectories for the other costs. The trajectory for J_2 has a small drop in the strain initially, but the control appears

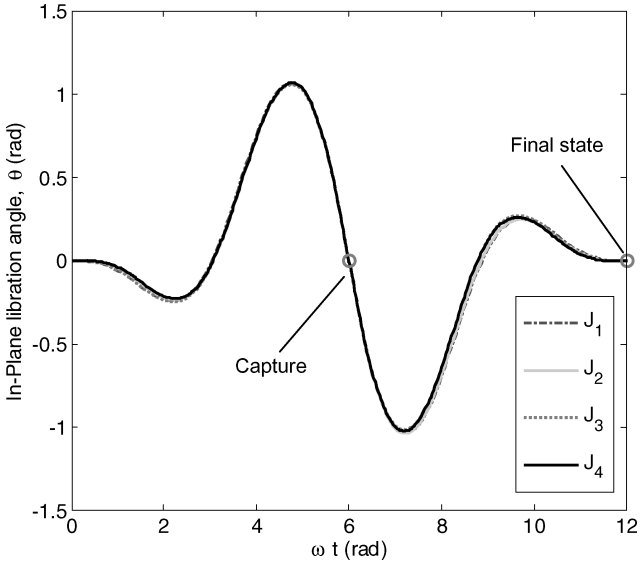

Fig. 5 Open-loop trajectories for in-plane libration angle.

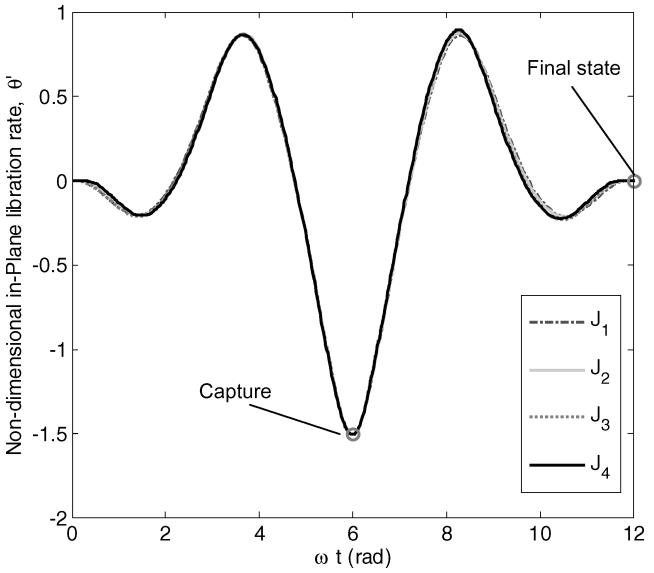

Fig. 6 Open-loop trajectory for nondimensional in-plane libration rate.

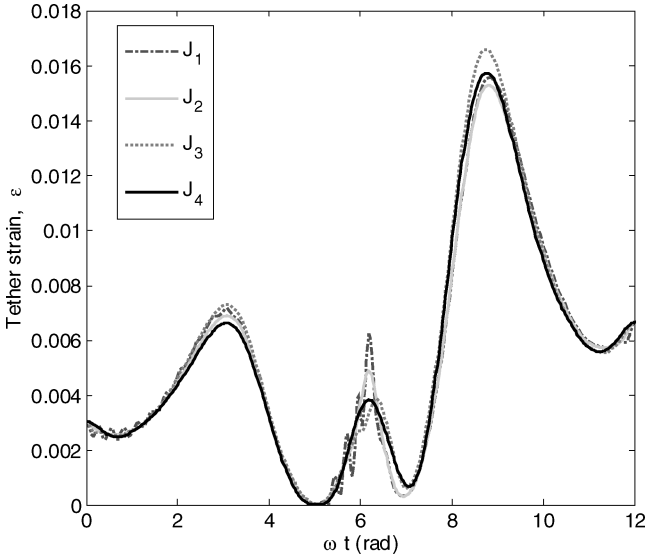

Fig. 7 Open-loop trajectory for tether strain.

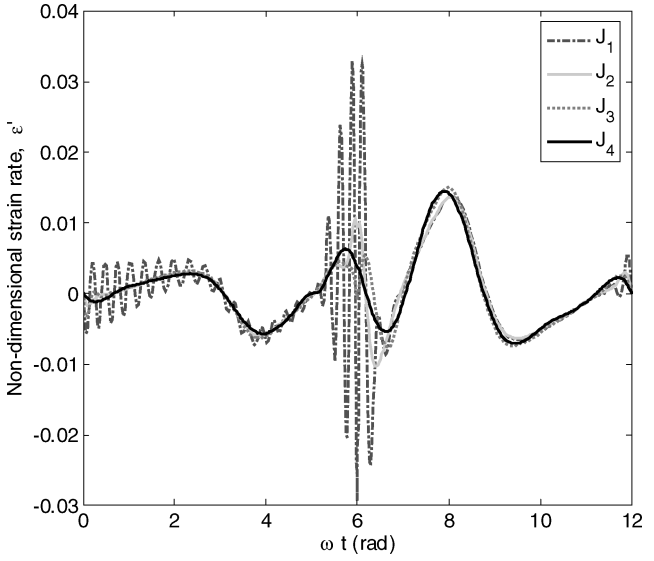

Fig. 8 Open-loop trajectory for nondimensional tether strain rate.

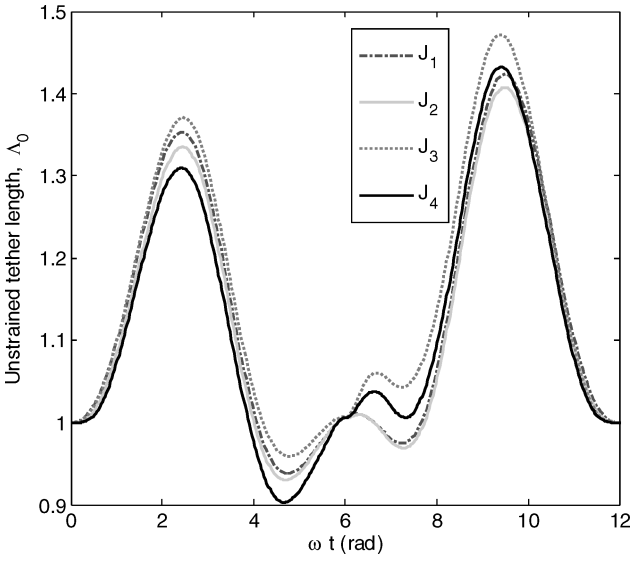

Fig. 9 Open-loop trajectory for nondimensional unstrained tether length.

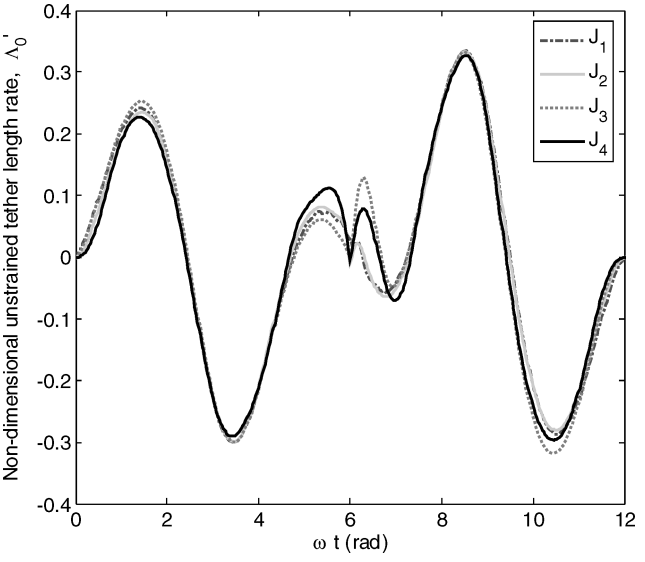

Fig. 10 Open-loop trajectory for nondimensional unstrained tether length rate.

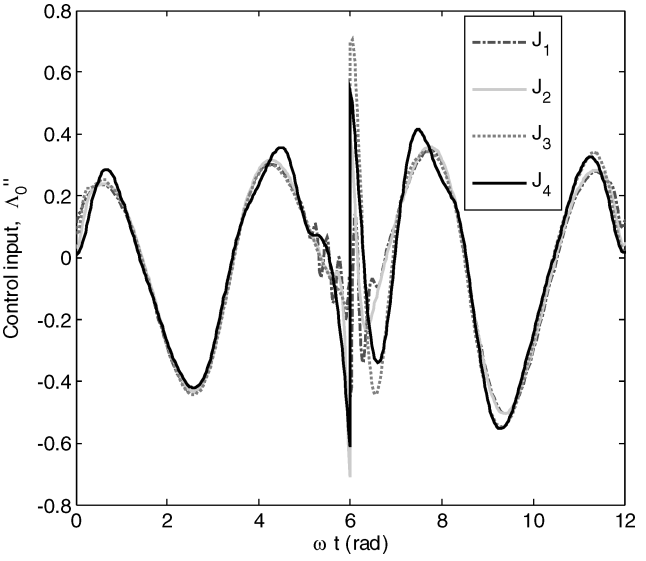

Fig. 11 Nondimensional control input (reel acceleration).

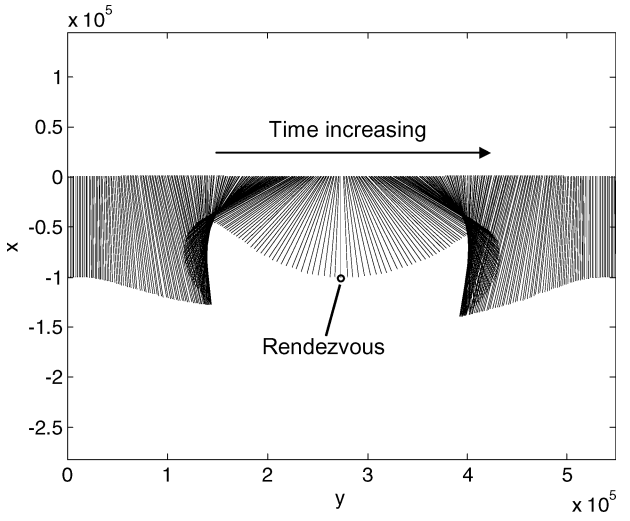

Fig. 12 Projections of tether configuration during payload capture maneuver (not to scale).

to damp this out very quickly. The variation in strain for each of the other costs is very smooth over the whole trajectory. The variation in strain magnitude over the trajectory is caused by the coupled effect of changes in tether length and the librational motion. (A positive libration rate acts to increase the tether tension, as does an increase in length.) The strain reduces to very low levels just before capture because of the large negative libration rate needed for payload capture. However, the strain is always positive, implying that the tether remains in tension. The most severe strain oscillations occur before payload capture for the cost J_1. The reason for this behavior is because the trajectory for J_1 penalizes only the control input in the first phase, not the longitudinal dynamics. Hence, a lower cost is achieved by pumping the longitudinal dynamics in the first phase to help mitigate the tension wave that would otherwise occur just following payload capture. Note that the variation in strain for J_1 in the second phase is very smooth. (It is also similar to the strain variation for J_2.) The final value, as well as the general amplitude of the strain in the second phase, is noticeably larger than the strain in the first phase. This is because of the added payload mass at the tether tip.

The tether strain rate, shown in Fig. 8, exemplifies the differences in the longitudinal dynamics for the different cost functions. The large longitudinal oscillations for the J_1 cost indicates that it is a rather poor choice for this maneuver. The trajectories for J_3 and J_4 are generally very smooth, although on the basis of strain rate, J_4 is the better of the two. It is also evident that the strain rate is not necessarily zero at the instant of capture. In fact, each different trajectory has a different strain rate at capture. This is allowable because the total radial velocity is still zero at the instant of capture as required by Eq. (16). It is clear that the optimal solution does not require the tether length rate and strain rate to be simultaneously zero at the capture point. This fact allows the postcapture dynamics to be damped so effectively without causing the tether to become slack. The most significant differences in the controllers are shown in Fig. 9, which shows the unstrained tether length. Figure 9 shows that the tether must be reeled-out, reeled-in, then reeled-out again to achieve the desired capture requirements. Although the overall variation in length is very similar for the different costs, the amount of deployed tether at any instant of time can be quite different (up to 8 km difference). In addition, the required tether length for capture is approximately 100 km, but to control the system fully for this particular maneuver requires a tether between 140 and 150 km in length.

The variation in length rate, shown in Fig. 10, illustrates that the main differences in the reel rate occur in the vicinity of the capture point. The reel requirements are generally also larger during the second phase than in the first. Note that one unit of nondimensional reel rate corresponds to approximately 110.7 m/s in dimensional units. Hence, the peak reel requirement is on the order of 36 m/s. The postcapture longitudinal oscillations are damped by reeling the tether out by a small amount following capture. One additional feature is that the derivative of the reel rate is discontinuous across the capture point. This is clearly visible in the reel acceleration trajectory shown in Fig. 11. The largest change in reel acceleration (jerk) occurs in the J_4 trajectory, followed by J_2. The smallest jerk occurs in the J_1 trajectory. Furthermore, the reel acceleration drops after capture for the J_1 trajectory, but increases for all other cost functions. The reason for the longitudinal vibrations in the J_1 trajectory is also evident by examining Fig. 11: The initial reel acceleration is the largest of all of the costs, and there is a deliberate pumping of the longitudinal mode in the 15 min before capture. Immediately following capture, the reel acceleration for J_1 has some higher frequency variations superimposed on the mean reel acceleration to help stabilize the postcapture vibrations. The other controllers are generally more well behaved than this. One unit of nondimensional reel acceleration is approximately 0.1225 m/s^2 in dimensional units. Therefore, the acceleration requirements for the reel are not too severe for this maneuver.

Projections of the tether at uniform instants of time are shown in Fig. 12 for the J_4 cost function. The maneuver is nearly symmetrical about the local vertical from a geometrical point of view, except for the longer tether length needed in the postcapture phase. Overall, the results illustrate the importance of selecting a physically desirable cost function for the maneuver. For example, if one used only J_1 as a measure, then it might be erroneously concluded that it is necessary to initiate large-amplitude longitudinal vibrations before payload capture. When the trajectories for the other cost functions are examined, it is clear that this is not the case. It appears that the minimum strain acceleration trajectory is the best in terms of maintaining smooth system dynamics and will be utilized in the remainder of the paper.

B. Closed-Loop Control

Even though the numerical methods used to generate the optimal control profiles are capable of producing results in times on the order of minutes, it is desirable to implement such solutions with an appropriate feedback strategy such that closed-loop stability can be demonstrated. Therefore, the open-loop controls could be stored, or even determined just before initiating the control actions, and a receding-horizon controller can be used to implement the required controls. This possibility is considered here. For simulations of the closed-loop system, the precapture and postcapture phases are treated separately. There are several good reasons for this. First, the precapture maneuver is strongly dependent on an accurate positioning of the tether tip to achieve rendezvous. Hence, strict terminal constraints must be placed on the tracking controller to give some reliance on its accuracy, particularly at the rendezvous time. Second, the postcapture phase is not as critical as the precapture phase, and so some tolerance is allowable on tracking the system states. More important, the exact mass of the object being captured may not be known, and so the tether strain determined from the open-loop controls may not be accurate. If terminal constraints were applied during this phase, then the control action may be erroneous, possibly leading to instability or a fatal control action. Therefore, no terminal constraints are applied in the postcapture phase. All system states are assumed to be measurable. The tether length and length rate are most easily measured. The libration angles could either be measured or estimated. The strain variation would be the most difficult to sense accurately, and a tensiometer would most likely be needed at the tether tip, rather than at the mother satellite, because the strain at the tip is critical for achieving the correct position.

1. *Precapture Phase*

Instead of performing an exhaustive study on the effect of horizon lengths, weighting matrices, and degree of discretization in the tracking controller, some reasonable values have been selected. The weighting matrices are selected as $\boldsymbol{Q} = 1000\boldsymbol{I}_{6\times 6}$ and $R = 10$. The horizon length has been selected as $T = 3$ rad, with the degree of discretization set as $N = 100$ for all simulations. There were 15

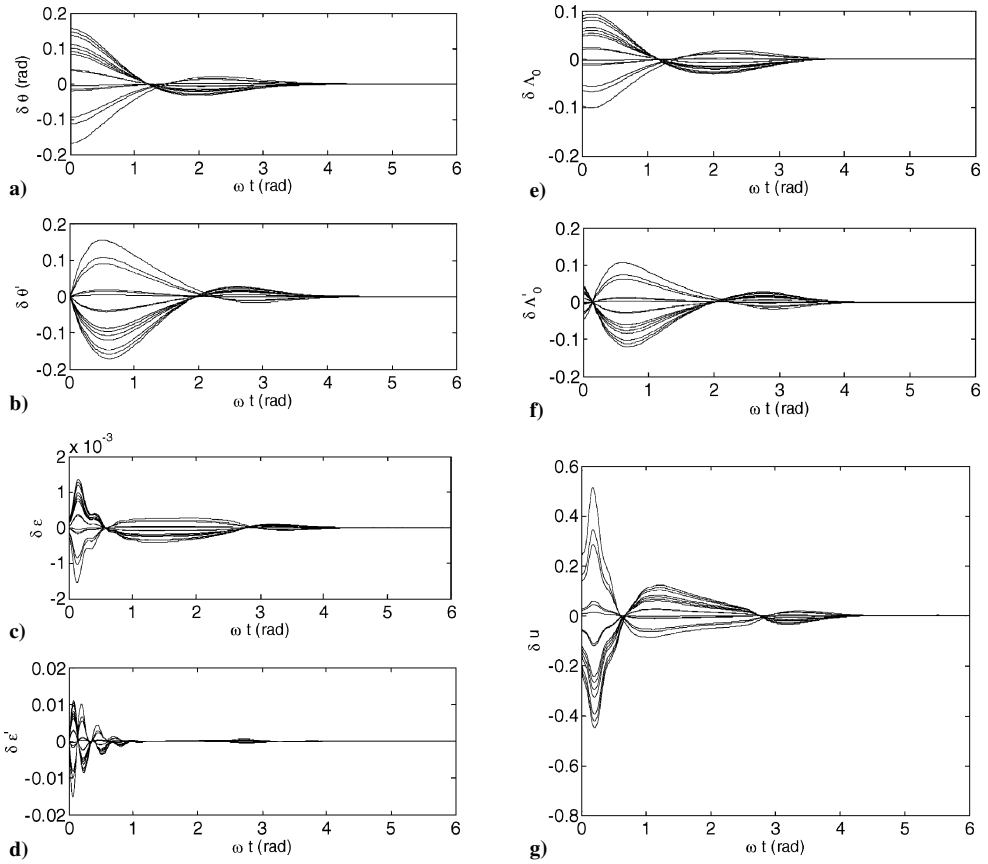

Fig. 13 Dispersions to system nondimensional state variables for precapture phase: a) in-plane libration angle, b) in-plane libration rate, c) strain, d) strain rate, e) unstrained tether length, f) unstrained tether length rate, and g) control input.

simulations performed using the receding-horizon controller with perturbations to the initial conditions. The perturbations to the initial conditions were distributed randomly within the ranges

$$|\Delta\theta(t_0)| \le 10 \text{ deg}, \qquad |\Delta\varepsilon(t_0)| \le 0.1\varepsilon(t_0)$$

$$|\Delta\Lambda_0(t_0)| \le 0.1, \qquad |\Delta\Lambda_0'(t_0)| \le 0.05 \tag{54}$$

All other states were kept as nominal. The perturbations given in Eq. (54) can be viewed as rather large disturbances in the context of a space tether system. They are far from the equilibrium values. Nevertheless, the perturbations serve to illustrate the effectiveness of the proposed closed-loop control.

Numerical results from the closed-loop simulations are shown in Fig. 13. Figure 13 shows the dispersions to the system state variables and control corrections required. This illustrates the excellent closed-loop performance of the system using only the reel acceleration as the control input. In particular, all system states converge to their desired values by the capture time. The required control corrections are shown in Fig. 13g, which shows that the control corrections are relatively smooth and keep the longitudinal vibrations stable. Note that, although not shown here, the closed-loop response for the tether strain remains positive at all instants of time. Furthermore, numerical simulations demonstrated that it is necessary to incorporate terminal constraints in the tracking controller. Without terminal constraints, the final position error of the tether tip is unacceptable. With terminal constraints, it can be seen that the tracking error is negligible at the final time. A comparison of Fig. 13d with Figs. 13b and 13f shows the large difference in the frequency of the longitudinal mode. The effect of this is evident in the feedback control shown in Fig. 13g, which has variations to control both the long- and short-period dynamics.

2. *Postcapture Phase*

To demonstrate the nature of the closed-loop performance for the postcapture phase, an additional 15 simulations were performed with the initial velocities following capture perturbed from their nominal values. It makes sense to only simulate perturbations to velocity because perturbations to position would mean that capture has not taken place. The applied perturbations were randomly dispersed in the ranges

$$|\Delta\theta'(t_1)| \le 0.05, \qquad |\Delta\varepsilon'(t_1)| \le 0.006, \qquad |\Delta\Lambda_0'(t_1)| \le 0.02 \tag{55}$$

In addition to errors in the capture velocity, uncertainties in the payload mass were also incorporated. The perturbations to the payload mass were randomly dispersed in the range

$$|\Delta m_2(t_1)| \le 200\,\text{kg} \tag{56}$$

which is a rather large (20%) error in the expected capture mass. Naturally, an uncertainty in the payload mass means that the equilibrium strain following capture will be different from the open-loop solution, and hence, the final values for the tether strain and tether length cannot be expected to match the nominal trajectory. Therefore, no terminal constraints are used in the postcapture phase.

Numerical results from closed-loop simulations of the postcapture phase are shown in Fig. 14. As expected, the dispersions to the tether strain and unstrained tether length do not approach zero, although their magnitudes are bounded and appear to approach constant magnitudes. This is indicated by the convergence of the strain rate and unstrained length rate to zero. The excellent closed-loop performance is demonstrated by examining the tether librational dispersions, as well as the dispersions to the system rates. For example, the dispersions to tether strain rate and unstrained tether length rate go to zero, indicating that any residual longitudinal vibrations caused by the errors in the payload mass have been damped. Furthermore, the total tether strain is always maintained above the lower limit, hence maintaining tether tension. The major difference between the closed-loop control of the second phase compared with the first is the significantly large control corrections required near

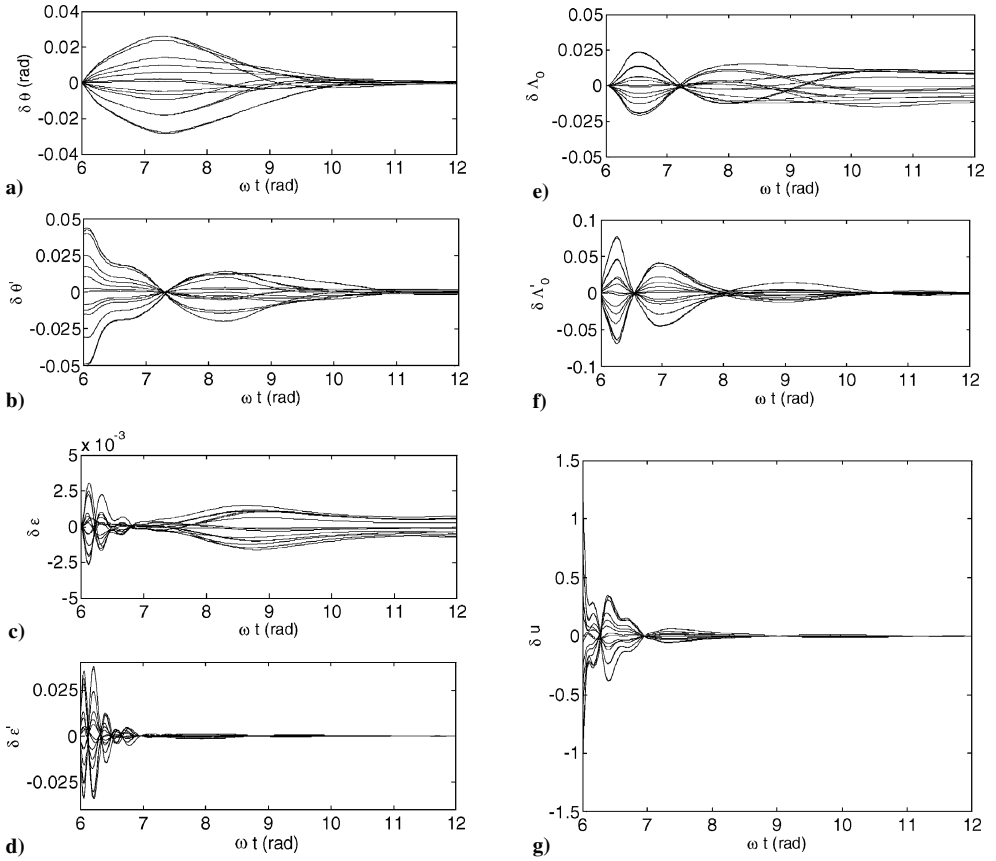

Fig. 14 Dispersions to system nondimensional state variables for postcapture phase, a) in-plane libration angle, b) in-plane libration rate, c) strain, d) strain-rate, e) unstrained tether length, f) unstrained tether length rate, and g) control input.

the beginning of the phase. These corrections are nearly double the maximum corrections required in the first phase.

The closed-loop simulations illustrate that it is possible to provide adequate feedback control for the system in both phases of the capture maneuver using only manipulation of the tether length. Important questions still remain, however, such as how to observe all of the system state variables and whether the system still performs as well in the presence of additional uncertainties (such as in the tether stiffness). Nevertheless, the results presented are extremely promising from the point of view of obtainable accuracy and the efficiency with which they can be generated.

VIII. Conclusions

An approach for controlling an elastic tether system for rendezvousing and capturing a payload has been presented. The optimal open-loop control law is determined by a direct Legendre pseudospectral method by treating the precapture and postcapture phases as a single, coupled maneuver. Treatment of tether elasticity offers advantages in specifying the rendezvous conditions at the tether tip that are not otherwise possible if the tether elasticity is neglected. Numerical results for a capture scenario in low Earth orbit clearly show that, in some cases, the precapture and postcapture phases are tightly coupled in the sense that control actions for damping the postcapture vibrations are initiated before capture. Numerical results also suggest the desirability to minimize the tether strain acceleration throughout the maneuver to reduce the tether longitudinal vibrations. Open-loop results illustrate the possibility of maneuvering the tether to rendezvous, capture, and damp postcapture vibrations using an integrated control methodology. Closed-loop control of the system using a receding-horizon strategy was also proposed. A receding-horizon controller based on the solution of a quadratic programming problem has been developed and can provide efficient and accurate solutions for time-varying reference trajectories. The closed-loop performance is excellent, even in the presence of large disturbances to the system states and uncertainties in the payload mass.

References

[1]Cosmo, M. L., and Lorenzini, E. C., *Tethers in Space Handbook*, 3rd ed., Smithsonian Astrophysical Observatory, Dec. 1997, Chap. 3.

[2]Smitherman, D. V., and Howell, J. T., "Space Elevators: Building a Permanent Bridge for Space Exploration and Economic Development," AIAA Paper 2000-5294, Sept. 2000.

[3]Nordley, G. D., and Forward, R. L., "Mars–Earth Rapid Interplanetary Tether Transport System: I. Initial Feasibility Analysis," *Journal of Propulsion and Power*, Vol. 17, No. 3, 2001, pp. 499–507.

[4]Eiden, M. J., and Cartmell, M. P., "Overcoming the Challenges: Tether Systems Roadmap for Space Transportation Applications," AIAA Paper 2003-2840, July 2003.

[5]Lorenzini, E. C., Bortolami, S. B., Rupp, C. C., and Angrilli, F., "Control and Flight Performance of Tethered Satellite Small Expendable Deployment System-II," *Journal of Guidance, Control, and Dynamics*, Vol. 19, No. 5, 1996, pp. 1148–1156.

[6]Misra, A. K., and Modi, V. J., "A Survey of the Dynamics and Control of Tethered Satellite Systems," *Advances in the Astronautical Sciences*, Vol. 62, Univelt, Inc., San Diego, CA, 1987, pp. 667–719.

[7]Williams, P., "Nonlinear Control and Applications of Tethered Space Systems," Ph.D. Dissertation, School of Aerospace, Mechanical, and Manufacturing Engineering, Royal Melbourne Inst. of Technology, Melbourne, Australia, April 2004.

[8]Johnson, L., Estes, R. D., Lorenzini, E. C., Martinez-Sanchez, M., Sanmartin, J., and Vas, I., "Electrodynamic Tethers for Spacecraft Propulsion," AIAA Paper 98-0983, Aug. 1998.

[9]Tragesser, S. G., and San, H., "Orbital Maneuvering with Electrodynamic Tethers," *Journal of Guidance, Control, and Dynamics*, Vol. 26, No. 5, 2003, pp. 805–810.

[10]Williams, P., "Optimal Orbit Transfer with Electrodynamic Tether," *Journal of Guidance, Control, and Dynamics*, Vol. 28, No. 2, 2005, pp. 369–372.

[11]Pearson, J., Levin, E., Carroll, J. A., and Oldson, J. C., "Orbital Maneuvering with Spinning Electrodynamic Tethers," AIAA Paper 2004-5715, Aug. 2004.

[12]Lorenzini, E. C., Cosmo, M. L., Kaiser, M., Bangham, M. E., Vonderwell, D. J., and Johnson, L., "Mission Analysis of Spinning Systems for Transfers from Low Orbits to Geostationary," *Journal of Spacecraft and Rockets*, Vol. 37, No. 2, 2000, pp. 165–172.

[13]Hoyt, R. P., and Uphoff, C., "Cislunar Tether Transport System," *Journal of Spacecraft and Rockets*, Vol. 37, No. 2, 2000, pp. 177–186.

[14]Kyroudis, G. A., and Conway, B. A., "Advantages of Tether Release of Satellites from Elliptic Orbits," *Journal of Guidance, Control, and Dynamics*, Vol. 11, No. 5, 1988, pp. 441–448.

[15]Ziegler, S. W., and Cartmell, M. P., "Using Motorized Tethers for Payload Orbital Transfer," *Journal of Spacecraft and Rockets*, Vol. 38, No. 6, 2001, pp. 904–913.

[16]Williams, P., Blanksby, C., and Trivailo, P., "Optimisation of Tether Assisted Sample Return from the International Space Station," Australian International Aerospace Congress, Paper AIAC 2003-021, 29 July–1 Aug. 2003.

[17]Williams, P., Blanksby, C., and Trivailo, P., "Tethered Planetary Capture Maneuvers," *Journal of Spacecraft and Rockets*, Vol. 41, No. 4, 2004, pp. 603–613.

[18]Longuski, J. M., Puig-Suari, J., and Mechalas, J., "Aerobraking Tethers for the Exploration of the Solar System," *Acta Astronautica*, Vol. 35, No. 2, 1995, pp. 205–214.

[19]Colombo, G., Gaposchkin, E. M., Grossi, M. D., and Weiffenbach, G. C., "The 'Skyhook': A Shuttle-Borne Tool for Low-Orbital-Altitude Research," *Meccanica*, March 1975, pp. 3–20.

[20]Lorenzini, E. C., Grossi, M. D., and Cosmo, M., "Low Altitude Tethered Mars Probe," *Acta Astronautica*, Vol. 21, No. 1, 1990, pp. 1–12.

[21]Sorensen, K. F., "Conceptual Design and Analysis of an MXER Tether Boost Station," 37th AIAA/ASME/SAE/ASEE Joint Propulsion Conf. and Exhibit, AIAA Paper 2001-3915, July 2001.

[22]Stuart, D. G., "Guidance and Control for Cooperative Tether-Mediated Orbital Rendezvous," *Journal of Guidance, Control, and Dynamics*, Vol. 13, No. 6, 1990, pp. 1102–1113.

[23]Blanksby, C., and Trivailo, P., "Assessment of Actuation Methods for Manipulating Tip Position of Long Tethers," *Space Technology, Space Engineering, Telecommunication, Systems Engineering and Control*, Vol. 20, No. 1, 2001, pp. 31–40.

[24]Williams, P., Blanksby, C., Trivailo, P., and Fujii, H. A., "In-Plane Payload Capture Using Tethers," *Acta Astronautica*, Vol. 57, No. 10, 2005, pp. 772–787.

[25]Williams, P., Blanksby, C., Trivailo, P., and Fujii, H. A., "Receding Horizon Control of Tether System Using Quasilinearisation and Chebyshev Pseudospectral Approximations," American Astronautical Society/AIAA Astrodynamics Specialists Conf., Paper AAS 03-535, Aug. 2003.

[26]Williams, P., "Spacecraft Rendezvous on Small Relative Inclination Orbits Using Tethers," *Journal of Spacecraft and Rockets*, Vol. 42, No. 6, 2005, pp. 1047–1060.

[27]Carroll, J. A., "Tether Applications in Space Transportation," *Acta Astronautica*, Vol. 13, No. 4, 1986, pp. 165–174.

[28]Carroll, J. A., "Preliminary Design for a 1 Km/Sec Tether Transport Facility," NASA Office of Aeronautics and Space Technology, Third Annual Advanced Propulsion Workshop, Jan. 1992.

[29]Williams, P., and Blanksby, C., "Prolonged Payload Rendezvous Using a Tether Actuator Mass," *Journal of Spacecraft and Rockets*, Vol. 41, No. 5, 2004, pp. 889–892.

[30]Westerhoff, J., "Active Control for MXER Tether Rendezvous Maneuvers," AIAA Paper 2003-5218, Aug. 2003.

[31]Misra, A. K., and Modi, V. J., "Deployment and Retrieval of Shuttle Supported Tethered Satellites," *Journal of Guidance, Control, and Dynamics*, Vol. 5, No. 3, 1982, pp. 278–285.

[32]Blanksby, C., Williams, P., and Trivailo, P., "Tether Assisted Rendezvous for Satellites with Small Relative Inclinations," 54th International Astronautical Congress, Paper IAC-03-A.P.09, 29 Sept.–3 Oct. 2003.

[33]Beletsky, V. V., and Levin, E. M., "Dynamics of Space Tether Systems," *Advances in the Astronautical Sciences*, Univelt, Inc., San Diego, CA, Vol. 83, 1993, Chap. 8.

[34]Branicky, M. S., Borkar, V. S., and Mitter, S. K., "A Unified Framework for Hybrid Control: Model and Optimal Control Theory," *IEEE Transactions on Automatic Control*, Vol. 43, No. 1, 1998, pp. 31–45.

[35]Barton, P. I., Banga, J. R., and Galan, S., "Optimization of Hybrid Discrete/Continuous Dynamic Systems," *Computers and Chemical Engineering*, Vol. 24, No. 9-10, 2000, pp. 2171–2182.

[36]Hedlund, S., and Rantzer, A., "Optimal Control of Hybrid Systems," *Proceedings of the 38th IEEE Conference on Decision and Control*, IEEE Publications, Piscataway, NJ, 1999, pp. 3972–3977.

[37]Sussman, H. J., "A Maximum Principle for Hybrid Optimal Control Problems," *Proceedings of the 38th IEEE Conference on Decision and Control*, IEEE Publications, Piscataway, NJ, 1999, pp. 425–430.

[38]Shaikh, M. S., and Caines, P. E., "On the Optimal Control of Hybrid Systems: Optimization of Trajectories, Switching Times, and Location Schedules," *Hybrid Systems: Computation and Control*, Springer-Verlag, Berlin, 2003, pp. 466–481.

[39]Ross, I. M., and Fahroo, F., "Pseudospectral Knotting Methods for Solving Optimal Control Problems," *Journal of Guidance, Control, and Dynamics*, Vol. 27, No. 3, 2004, pp. 397–405.

[40]Bryson, A. E., and Ho, Y. C., *Applied Optimal Control*, Hemisphere, New York, 1975, Chap. 7.

[41]Betts, J. T., *Practical Methods for Optimal Control Using Nonlinear Programming*, SIAM Advances in Control and Design Series, Society for Industrial and Applied Mechanics, Philadelphia, PA, 2001, Chap. 4.

[42]Hargraves, C. R., and Paris, S. W., "Direct Trajectory Optimization Using Nonlinear Programming and Collocation," *Journal of Guidance, Control, and Dynamics*, Vol. 10, No. 4, 1987, pp. 338–342.

[43]Herman, A. L., and Conway, B. A., "Direct Optimization Using Collocation Based on High-Order Gauss–Lobatto Quadrature Rules," *Journal of Guidance, Control, and Dynamics*, Vol. 19, No. 3, 1996, pp. 592–599.

[44]Elnagar, G., Kazemi, M. A., and Razzaghi, M., "The Legendre Pseudospectral Method for Discretizing Optimal Control Problems," *IEEE Transactions on Automatic Control*, Vol. 40, No. 10, 1995, pp. 1793–1796.

[45]Ross, I. M., and Fahroo, F., "Legendre Pseudospectral Approximations of Optimal Control Problems," *Lecture Notes in Control and Information Sciences*, Vol. 295, Springer-Verlag, Berlin, 2003, pp. 327–342.

[46]Williams, P., "User's Guide to DIRECT Version 1.18," Technical Rept. TR-0301.01, School of Aerospace, Mechanical, and Manufacturing, Royal Melbourne Instiute of Technology, Melbourne, Australia, Jan. 2006.

[47]Gill, P. E., Murray, W., and Saunders, M. A., "SNOPT: An SQP Algorithm for Large-Scale Constrained Optimization," *SIAM Journal on Optimization*, Vol. 12, No. 4, 2002, pp. 979–1006.

[48]Williams, P., and Trivailo, P., "On the Optimal Deployment and Retrieval of Tethered Satellites," AIAA Paper 2005-4291, July 2005.

[49]Lu, P., "Regulation About Time-Varying Trajectories: Precision Entry Guidance Illustrated," *Journal of Guidance, Control, and Dynamics*, Vol. 22, No. 6, 1999, pp. 784–790.

[50]Williams, P., "Application of Pseudospectral Methods for Receding Horizon Control," *Journal of Guidance, Control, and Dynamics*, Vol. 27, No. 2, 2004, pp. 310–314.

[51]Yan, H., Fahroo, F., and Ross, I. M., "Real-Time Computation of Neighboring Optimal Control Laws," AIAA Paper 2002-4657, Aug. 2002.

[52]Fletcher, R., *Practical Methods of Optimization*, 2nd ed., Wiley, New York, 1989, Chap. 10.